Reaction Force Control of a Linear Electrical Generator for Direct Drive Wave Energy Conversion

Reaction Force Control of a Linear Electrical Generator for Direct Drive Wave Energy Conversion

Jonathan K.H. Shek[1], D. Ewen Macpherson[1], Markus A. Mueller[1], and Jianping Xiang[2]

[1] Institute for Energy Systems, School of Engineering and Electronics, The University of Edinburgh, The King's Buildings, Mayfield Road, Edinburgh, EH9 3JL, United Kingdom.

[2] Department of Electronic and Electrical Engineering, Loughborough University, Loughborough, Leicestershire, LE11 3TU, United Kingdom

Email : j.shek@ed.ac.uk

Abstract: Direct drive wave energy converters have been proposed in view of the disadvantage of mechanical complexity and low conversion efficiencies in conventional wave energy converters. By directly coupling a linear generator to a reciprocating wave energy device it is suggested that direct drive power take-off could be a viable alternative to hydraulic and pneumatic based systems. To further realise the benefits of a direct drive system this paper presents a control scheme based on reaction force control to maximise energy extraction. It focuses predominantly on the theoretical analysis of the linear generator reaction force. The modelling, simulation and control of direct drive wave energy conversion are systematically investigated by computer-aided analysis via Matlab/Simulink.

1 Introduction

Wave energy has the potential to make a significant contribution in reducing carbon emissions with targets set by the UK government in a 2003 White Paper [1]. The energy from waves in UK waters represents half of Europe's total wave resource; the technical resource is estimated at approximately one quarter of the UK's total installed generation capacity [2]. Developments in wave energy conversion have concentrated on the method of extraction rather than the electrical power conversion. As a consequence, power take-off systems that make use of conventional high speed rotary electrical generators such as induction machines and synchronous machines have been implemented in wave energy converters (WECs). Direct drive power take-off systems incorporating linear generators have been proposed as a viable alternative to the use of conventional rotating machines [3, 4]. By utilising linear generators that operate at low speed, the need for a mechanical interface involving complex hydraulic or pneumatic systems is eradicated, resulting in a simpler power take-off system with fewer conversion losses. An example where a direct drive power take-off system has been used can be found in the Archimedes Wave Swing (AWS) WEC [5].

The reciprocating motion of a linear generator implies that direct drive power take-off systems can be implemented in point absorber or heaving buoy type WECs by direct coupling, as shown in Fig. 1. The frequency at which sea waves excite a wave energy device can vary enormously, but the capture bandwidth of a device is limited. Point absorbers naturally have a narrow bandwidth due to their small physical dimensions compared to the incident wavelength. Therefore, device characteristics need to be matched to the wave climate so that maximum energy can be extracted from the waves. This makes it essential to control the reciprocating motion of a wave energy device if they are to work well over a wide range of conditions.

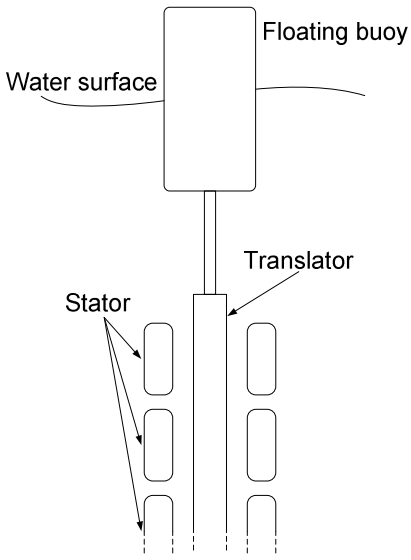

Fig. 1 *Diagram of a generic direct drive wave energy converter*

A number of investigators have proposed various methods for achieving control; most of which aim to obtain an optimum phase and optimum amplitude of oscillation to maximise the energy extracted [6-8]. In each case a purely mechanical or electro-mechanical method was suggested.

In this paper the authors present a method of controlling a heaving buoy point absorber by utilising a linear electrical generator directly coupled to a wave energy device. The paper begins with an overview of a heaving buoy point absorber coupled to a linear electrical generator. The parameters for phase and amplitude control are expressed in electrical terms. It then explains how the generator reaction force can be used to control these parameters through armature current control. The paper then focuses on the development of a direct drive WEC model with control implementation which, in particular, emphasises the generator reaction force production for a linear vernier hybrid machine. Simulation results from the model are presented for control in regular seas. Linear theory of point absorbers under monochromatic wave-excitation is assumed throughout the paper.

2 Control of Point Absorbers

A point absorber can be represented using the electrical analogue of a mass spring damper system to give an insight into power transfer within a direct drive WEC [9]. Figure 2 shows a series resonant circuit representing the wave energy device and generator where the electrical equivalent of the wave excitation force (F_e) is represented by an EMF source. The EMF source drives an equivalent current, the device velocity (U) through the various elements of the circuit: inductance represents the mass of the device (M), capacitance is the inverse of the spring stiffness force constant (K_w) and the resistance is the mechanical damping (B_w) which includes radiation resistance due to the radiation of waves by the oscillating body. The load represents the generator, having a reaction force (F_g) across an equivalent variable and controllable impedance (Z_g). Frictional losses from the generator are also represented by Z_g.

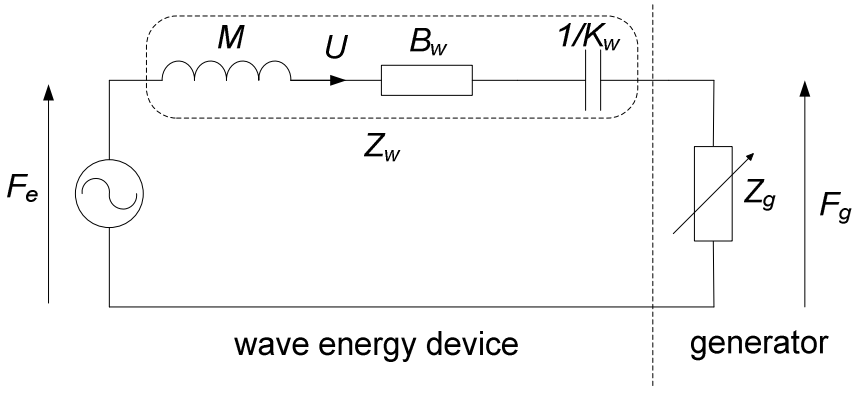

Fig. 2 *Electrical analogue of a point absorber*

The expression for the device impedance (Z_w) is given by applying electrical theory to the circuit in Fig. 2.

$$Z_w = B_w + j\omega M - j\frac{K_w}{\omega} \qquad (1)$$

By expanding the load impedance (Z_g) in terms of equivalent resistive, inductive or capacitive components, the ability of the generator to control the frequency characteristics of the above circuit can be investigated. As with an electrical circuit the forces can be represented by a phasor diagram as shown in Fig. 3 where it is assumed that the displacement $x(t)$ is given by (2).

$$x = X\sin(\omega t + \varphi_x) \qquad (2)$$

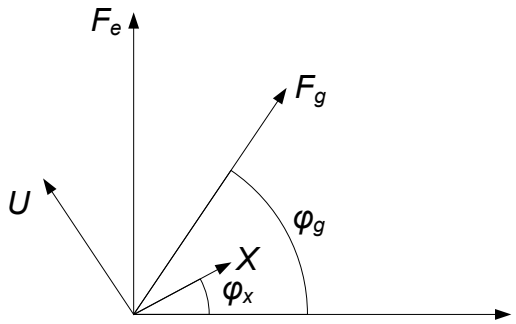

Fig. 3 *Phasor representation of excitation and generator forces at frequency ω*

The generator reaction force and the excitation force are given by (3) and (4) respectively.

$$f_g = F_g\sin(\omega t + \varphi_g) \qquad (3)$$

$$f_e = F_e\cos(\omega t) \qquad (4)$$

By using trigonometric identities the generator force can be represented by two force terms: one which is proportional to velocity, and a second force term that is proportional to displacement. These forces can be represented by a damping force term ($B_g\dot{x}$) and a spring force term ($K_g x$) respectively as shown in (5). The generator impedance (Z_g) can therefore also be represented as a damping component and a spring stiffness component as shown in (6) and in Fig. 4.

$$f_g = B_g\dot{x} + K_g x \qquad (5)$$

$$Z_g = B_g - j\frac{K_g}{\omega} \tag{6}$$

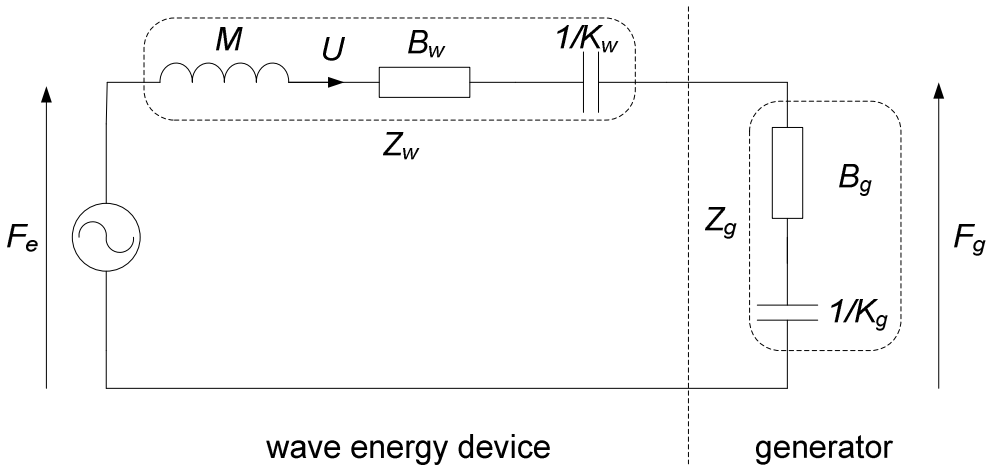

Fig. 4 *Electrical analogue of a point absorber wave energy converter, with Z_g represented as damping and spring stiffness components*

Similarly to an electrical series resonant circuit, mechanical resonance occurs in a point absorber WEC when the sum of the imaginary components of the total impedance adds up to zero. Maximum power transfer occurs when the generator impedance is equal to the complex conjugate of the device impedance. Hence, the generator impedances have to be controlled to meet the following requirements given in (7) and (8) to achieve amplitude and phase control:

$$B_g = B_w \tag{7}$$

$$\frac{K_g}{\omega} = \omega M - \frac{K_w}{\omega} \tag{8}$$

In a linear electrical generator phase control requires the control of a force that emulates a spring stiffness force. Amplitude control requires control of a force similar to a damping force.

$$\omega_0 = \sqrt{\frac{(K_w + K_g)}{M}} \tag{9}$$

The resonant frequency is given in (9) which can be controlled by varying the generator spring stiffness constant. At resonance the total impedance of the point absorber and the load is real; the excitation force (F_e) and the velocity (U)

are in phase, and therefore, maximum power is transferred to the load impedance which represents the generator. This is shown in Fig. 5 where the phase of the load at resonance (φ_g) is given by (10).

$$\varphi_g = \tan^{-1}\left(-\frac{K_g}{B_g \omega}\right) \tag{10}$$

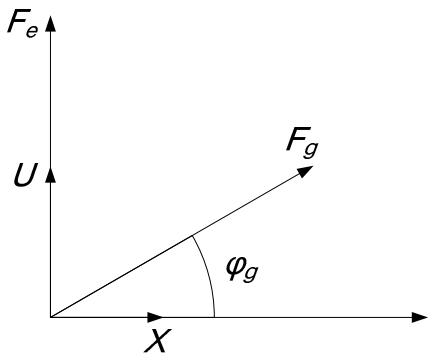

Fig. 5 *Phasor representation of excitation and generator forces at resonance*

3 Implementation of Phase and Amplitude Control

In order to control the phase and amplitude of a heaving point absorber, the force generated by a directly coupled linear electrical generator, the so-called generator reaction force, can be utilised. The generator force can be represented as two components: a damping force proportional to velocity and a spring stiffness force proportional to displacement, as given in (5). The generator force is a function of the geometry and properties of the permanent magnets, the machine design and the peak current. However, only the latter can be used to control this force. Therefore, in order to resolve the generator force vector (f_g) into two orthogonal components, the current vector is decomposed into the x - directed component and the $\dot{x}$ -directed component.

$$f_g = \frac{3}{2} K_{\hat{F}} \hat{I} \cos(\omega t + \varphi_g) \tag{11}$$

The expression for generator force given in (11) which is derived in section 4 can be expanded to give:

$$f_g = \frac{3K_{\hat{F}}}{2}\left(\hat{I}\cos\omega t\cos\varphi_g - \hat{I}\sin\omega t\sin\varphi_g\right) \tag{12}$$

where the two current terms in the brackets can be represented as current phasors i_x and $i_{\dot{x}}$. Electrically, these are the orthogonal components of the armature current envelope. A simplified equation is shown in (13) where $K_G = \frac{3K_{\hat{F}}}{2}$, $i_x = -\hat{I}\sin\varphi_g \sin\omega t$ and $i_{\dot{x}} = \hat{I}\cos\varphi_g \cos\omega t$.

$$f_g = K_G (i_x + i_{\dot{x}}) \tag{13}$$

By comparing (5) and (13) expressions can be given for the generator forces in terms of the damping and spring stiffness forces. These are given in (14a) and (14b) which can be rearranged to provide the current vector requirements in terms of the generator spring stiffness and damping constants shown by the equations in (15) which can also be expressed in terms of the device parameters as described in section 2.

$$f_{gx} = -K_g x = i_x K_G \tag{14a}$$

$$f_{g\dot{x}} = B_g \dot{x} = i_{\dot{x}} K_G \tag{14b}$$

$$i_x = -\left(\frac{K_g}{K_G}\right)x \tag{15a}$$

$$i_{\dot{x}} = \left(\frac{B_g}{K_G}\right)\dot{x} \tag{15b}$$

Subsequently, the desired 3-phase currents are derived from the current vectors and used for current regulation.

By controlling the current vectors i_x and $i_{\dot{x}}$ it is therefore possible to control the phase and amplitude of the device for maximum energy conversion. The current vector i_x controls the generator spring stiffness force providing phase control; the current vector $i_{\dot{x}}$ controls the damping force providing amplitude control and conversion of real power.

4 Direct Drive Wave Energy Converter Model

A direct drive WEC was modelled using Matlab/Simulink. A description of the model is given in 4.1, followed by an in-depth description of the generator reaction force model in 4.2.

4.1 Simulink Model Description

Figure 6 shows a Simulink model of a direct drive WEC. The model primarily comprises a wave energy capture device modelled as a mass-spring-damper system and a power take-off system that includes the linear generator, the power converter and the control system.

The linear generator is modelled on the vernier hybrid machine (VHM) [10, 11] which is based on the Variable Reluctance Permanent Magnet (VRPM) machine topology. VRPM machines are well known to have high shear

stresses and are particularly suited to low speed, high torque applications. Shear stresses of up to 200 kN/m^2 can be found in machines such as the Transverse Flux Permanent Magnet machine, but resulting in low power factor and construction complexity. The VHM goes some way to resolving the latter by adopting a more conventional machine structure.

The electrical output of the linear generator has variable amplitude and frequency due to the reciprocating motion of the point absorber. The model uses two back-to-back inverters for the power conversion stage to allow inversion into the mains and armature current control by way of active rectification. A description of the converter design and operation can be found in [12].

The control system implements the control procedure described in the previous section and is divided into two main subsystems within the power take-off block, which is shown in Fig. 7. The spring stiffness and damping coefficient requirements are used to calculate the x - directed and $\dot{x}$ - directed current components, which are then fed into the 1st subsystem (3-phase i) to derive the required 3-phase armature currents. The required 3-phase currents are then compared with the actual 3-phase currents by a 2nd subsystem (i control); the error is used to generate driving signals for the power converter switches on the active rectifier side. A similar controller exists to regulate the DC link voltage via the inverter, which has a direct influence on the rate of change of the armature currents. A well maintained DC link voltage would not only allow the armature current to be controlled effectively, but would in turn allow the motion of the point absorber to be more in tune with the incident wave.

Hydrodynamic parameters are required in both the wave energy capture device model and the power take-off model where numerical values are calculated based on a method described in Eidsmoen, using linear hydrodynamic theory [13]. These numerical values are subsequently stored in look-up tables as excitation force, added mass and damping coefficients, which are then used to derive the excitation force due to the incident wave and the radiation impedance, which make up the added mass and damping forces.

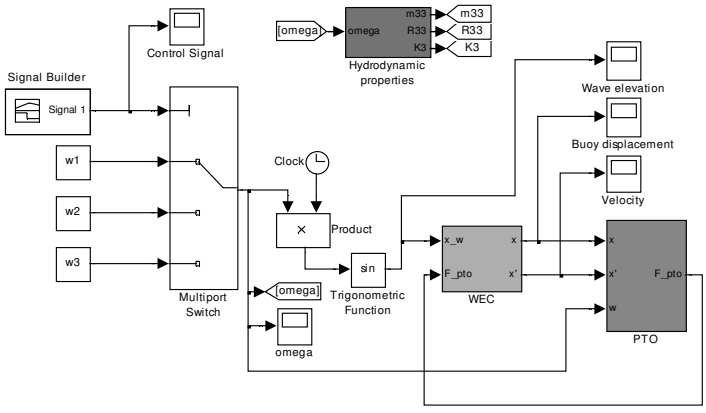

Fig. 6 *Simulink model of a direct drive wave energy converter with implementation of phase and amplitude control*

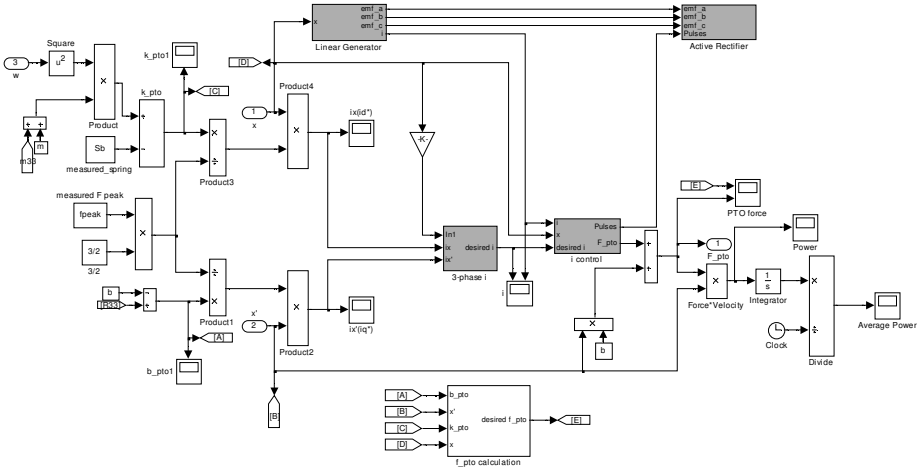

Fig. 7 *Simulink model of the power take-off (PTO) block*

4.2 Generator Reaction Force Model

As with a conventional electrical machine, the useful force in a linear machine is produced by the interaction of current carrying conductors with a magnetic field known as the Lorentz force. If the magnetic field (B) and the current (I) in a conductor of length l are perpendicular, the Lorentz force is given by (16) where q is the charge travelling along a conductor at a velocity v.

$$F = qvB = IlB \tag{16}$$

Calculation of the Lorentz forces in an electrical machine can be achieved using finite element modelling with a reasonable level of confidence. The force can be stored in a look-up table for various positions of the translator in the machine and then used in the control simulation. However, a new finite element model has to be regenerated for any change in geometry and so is not very versatile for use in the design office. Hence a simpler analytical model is derived and presented in this paper with finite element and experimental results to support the model.

A cross-section of one phase of a linear VHM is shown in Fig. 8(a). A linear toothed translator moves back and forth between two C-cores with coils wound on each pole. Magnets are mounted on each pole face so that the flux flow is of that shown in Fig. 8(a) when the translator teeth are fully aligned with the magnets. The flux decays to zero and then reverses polarity as the translator moves to the fully unaligned position. Hence, the coils experience a rapid change in flux where the electrical frequency of the pulsations is greater than the frequency of translator oscillation, producing a so-called magnetic gearing effect. For a 3-phase machine the adjacent phases are separated by two thirds of a translator pitch so that the flux pulsations are 120 degrees out of phase. The machine can be constructed via a modular approach with each phase magnetically isolated from the other, which allows a high degree of flexibility in the choice

of power ratings and design parameters. Details of the design and modelling of the linear machine can be found in references [14, 15].

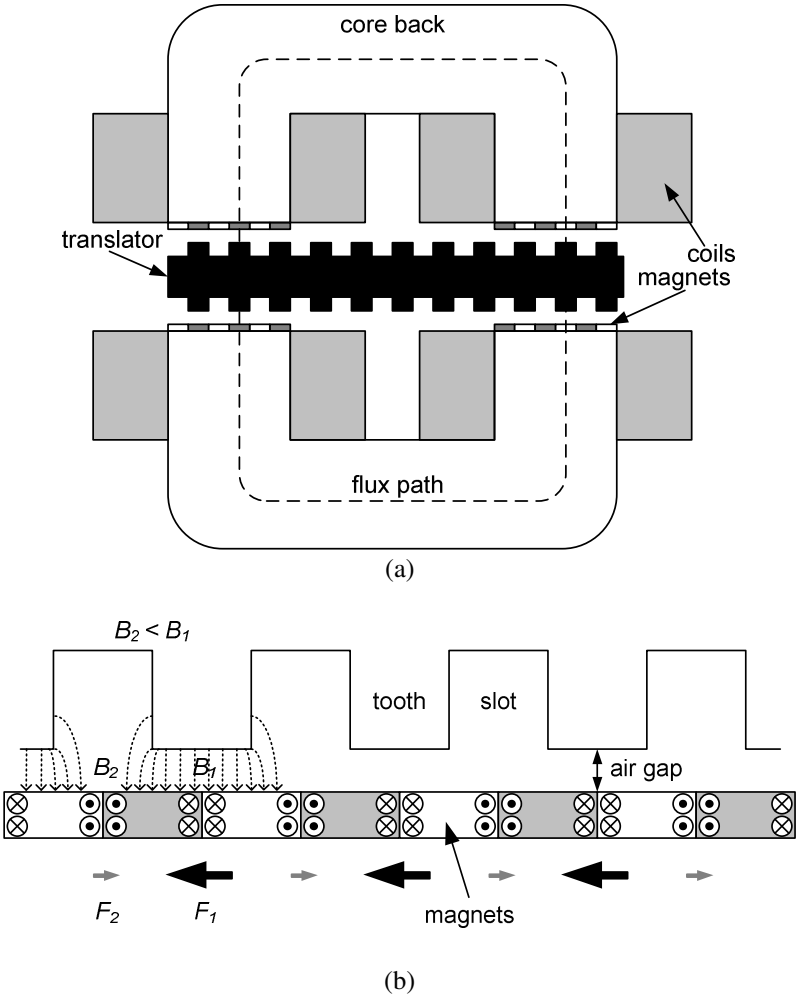

Fig. 8 (a) One phase module of the linear VHM, (b) Method of force production

Figure 8(b) shows the machine magnified around one pole face to illustrate the method of force production. A set of equivalent currents is used to represent the permanent magnets mounted on the pole face with the magnetic field produced by the coils wound around each limb of the C-core. A higher flux density (B_1) is observed in the air gap under a tooth compared to the flux density in the slot region (B_2). As shown in the diagram maximum force is produced when the centre of the tooth is aligned with the interface between two adjacent magnets. If the magnetic field is in the direction shown, a large force is produced under a tooth (F_1) and a smaller force acting in the opposite direction is produced in the slot region (F_2). The peak force on one translator tooth is given by:

$$\hat{F}_{tooth} = (B_1 - B_2) I_{PM} l \qquad (17)$$

where B_1 and B_2 are both due to the armature excitation, l is the core length of the machine and I_{PM}, given in (18), is the equivalent current at the interface of two adjacent magnets of thickness t.

$$I_{PM} = \frac{2B_{rem}t}{\mu_0\mu_r} \tag{18}$$

B_{rem} is the remanent flux density of the rare-earth magnets, μ_0 is the permeability of free space and μ_r is the permanent magnet recoil permeability. A conformal transformation technique has been applied by Spooner and Haydock [10] to calculate B_1 & B_2 and is given in (19).

$$\frac{B_2}{B_1} = \frac{g}{\sqrt{g^2 + a^2}} \tag{19}$$

where a is half the slot width, and g is the distance between the translator and the pole face and is equal to the sum of the actual air gap length and the so-called magnetic air gap. Hence, the peak force for one phase with p pole faces and Z teeth per face can now be re-written as:

$$\hat{F}_{phase} = pZB_1\left(1 - \frac{g}{\sqrt{g^2 + a^2}}\right)I_{PM}\,l \tag{20}$$

The maximum flux density (B_1) is given in (21). It is calculated from the magnetic reluctance network of one phase with the assumption that the magnetic air gap is constant.

$$B_1 = N\frac{\mu_0}{g}i_A(t) \tag{21}$$

where N is the number of turns per coil and $i_A(t)$ is the coil armature current which can be controlled. A similar expression has been derived by Iwabuchi et al [16] with the only difference being that their expression for peak force contains a constant, β, which is equal to the bracketed term in (20).

As the translator moves position, the flux density waveform produced by the armature currents moves with the translator, so that the force acting on the translator teeth changes also. The geometry of the air gap was chosen for an example machine such that the harmonics in the flux density waveform can be ignored [17]. Hence, the flux density waveform in the air gap is assumed to be sinusoidal; so, it can be inferred that the force distribution with position is also sinusoidal. For a translator oscillation frequency, ω, which would be equal to the buoy frequency in a direct drive system the force for a single phase machine is given by (22).

$$f(x,t) = K_{\hat{F}} \sin 2\pi\left(\frac{x}{\lambda} - \omega t\right)i_A(t) \tag{22}$$

where the peak force constant is given by

$$K_{\hat{F}} = pZ\left(1 - \frac{g}{\sqrt{g^2 + a^2}}\right) I_{PM} lN \frac{\mu_0}{g} \tag{23}$$

In most applications there will be three phases each producing its own force similar to (22), but each force will be out of phase with the other by 120 electrical degrees. The form of the phase current depends upon the nature of the induced EMF, which is given by (24) to (26) for all three phases [12].

$$e_A = \hat{E}\cos(\frac{2\pi}{\lambda}x + \theta_0)\cos(\omega t + \varphi_g) \tag{24}$$

$$e_B = \hat{E}\cos(\frac{2\pi}{\lambda}x - \frac{2\pi}{3} + \theta_0)\cos(\omega t + \varphi_g) \tag{25}$$

$$e_C = \hat{E}\cos(\frac{2\pi}{\lambda}x + \frac{2\pi}{3} + \theta_0)\cos(\omega t + \varphi_g) \tag{26}$$

In order to convert maximum electrical power from the linear VHM the induced EMF and the current must be in phase with one another in order to compensate for the high reactance typical of these machines. Hence, the phase currents will be of a similar form to the induced voltages and are given in (27) to (29).

$$i_A = \hat{I}\cos(\frac{2\pi}{\lambda}x + \theta_0)\cos(\omega t + \varphi_g) \tag{27}$$

$$i_B = \hat{I}\cos(\frac{2\pi}{\lambda}x - \frac{2\pi}{3} + \theta_0)\cos(\omega t + \varphi_g) \tag{28}$$

$$i_C = \hat{I}\cos(\frac{2\pi}{\lambda}x + \frac{2\pi}{3} + \theta_0)\cos(\omega t + \varphi_g) \tag{29}$$

Substituting each of the 3-phase currents into (22) will produce the forces produced by each phase. The total reaction force generated by the machine is equal to the sum, which is expressed in (30) and assumes that $\theta_0 = \pi/2$.

$$f_g = \frac{3}{2} K_{\hat{F}} \hat{I}\cos(\omega t + \varphi_g) \tag{30}$$

For a point absorber in monochromatic waves the excitation force is assumed to be in phase with the wave displacement. Hence, the generator force is of a similar distribution to the excitation force enabling it to be used to control the point absorber. Equation (30) only includes the electromagnetic force due to Lorentz. However, even with no current flowing, a force exists due to the alignment of the magnets with the teeth on the translator; a so called cogging force. In this machine it was found that provided the machine is balanced, the cogging forces produced by each phase were distributed such that their sum was always equal to zero.

In order to verify this force model force calculations from a finite element model were generated. The finite element model was verified using experimental results of a prototype machine in reference [15], in which full details of the finite element model can be found. Figure 9 shows a comparison between the two sets of force data.

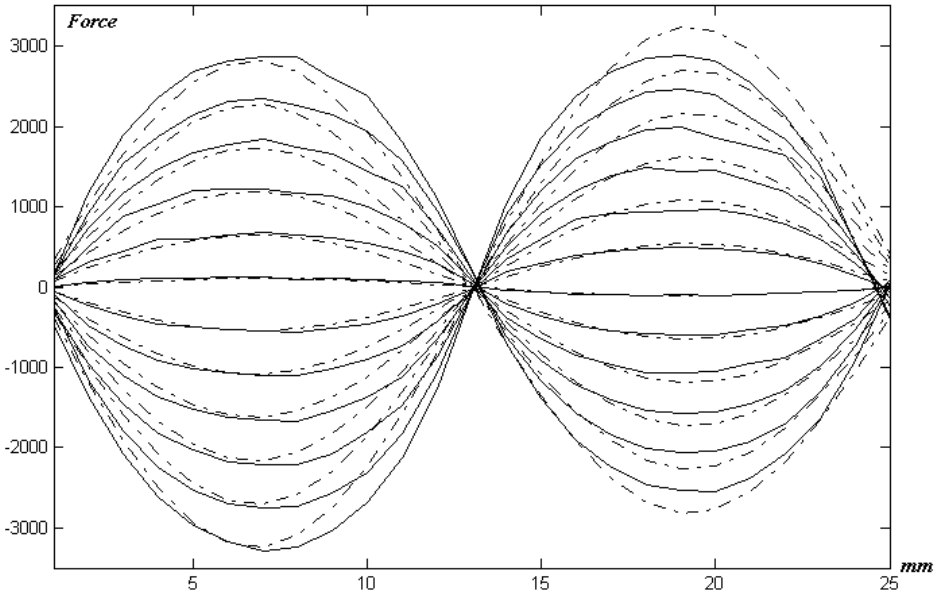

Fig. 9 Comparison between finite element force data (solid line) and the force model data (dotted line)

5 Results

Simulation results are based on a model of a linear generator directly coupled to a floating buoy with a single degree-of-freedom. The floating buoy is excited by a sinusoidal wave force at a frequency of 1.3 rad/s, causing it to exhibit heave motion. Parameters related to the simulations can be found in Table 1.

Figure 10(a) shows the frequency response for an uncontrolled direct drive WEC. As expected, average power is at a maximum when the wave excitation frequency coincides with the natural frequency of the WEC. On either side of the natural frequency the extracted power rapidly decreases. In Fig. 10(b) the velocity of a controlled heaving buoy is in phase with the wave excitation force so that maximum power can be extracted from the waves. This is achieved by calculating the required spring stiffness and damping to be produced by the generator, which is controlled by the x-directed and the $\dot{x}$-directed current components, i_x and $i_{\dot{x}}$, as shown in Fig. 10(c). For this particular simulation, the required generator spring stiffness force is much greater than the required generator damping force. Hence, i_x has a greater amplitude in comparison to $i_{\dot{x}}$. The envelope of the 3-phase currents given by $i_x + i_{\dot{x}}$ in which i_x dominates is therefore out of phase with the envelope of the induced EMF, where EMF is proportional to the velocity of the heaving buoy, as shown in Fig. 10(d) and Fig. 10(e). This implies that generator power flow is not unidirectional due to the reactive power demands in order to achieve mechanical resonance. Indeed, any amount of spring stiffness produced by the linear generator would mean that electrical resonance is not achieved. This is simply due to the i_x component that is required for energy to be returned to the sea for part of the cycle. The only condition where mechanical and electrical

resonance can be achieved simultaneously is when the linear generator is not required to produce a spring stiffness force, and therefore, only the $i_{\dot{x}}$ component exists, which allows the armature currents to be in phase with the induced EMF. In Fig. 10(f) the instantaneous power produced by the linear generator has a peak value of about 375 kW, whereas the average power is around 70 kW. As a result, the linear generator and power converter would have to be considerably overrated for maximum power extraction. However, measures can be taken to reduce the level of overrating that would still result in a vast improvement in extracted wave power compared with an uncontrolled system. Implementing these measures would also allow direct drive WECs to be optimised for specific requirements that are not necessarily based on extracting maximum power from each WEC. Ongoing investigations into different approaches are being explored along with extension to real seas states.

Table 1: Simulation parameters

Wave excitation frequency	1.3 rad/s
Natural frequency of the point absorber WEC	1.4 rad/s
Mass of floating buoy	48383 kg
Hydrostatic spring stiffness	126230 N/m
Hydrodynamic damping	3032 Ns/m
Generator spring stiffness	-18291 N/m
Generator damping	2884.26 Ns/m

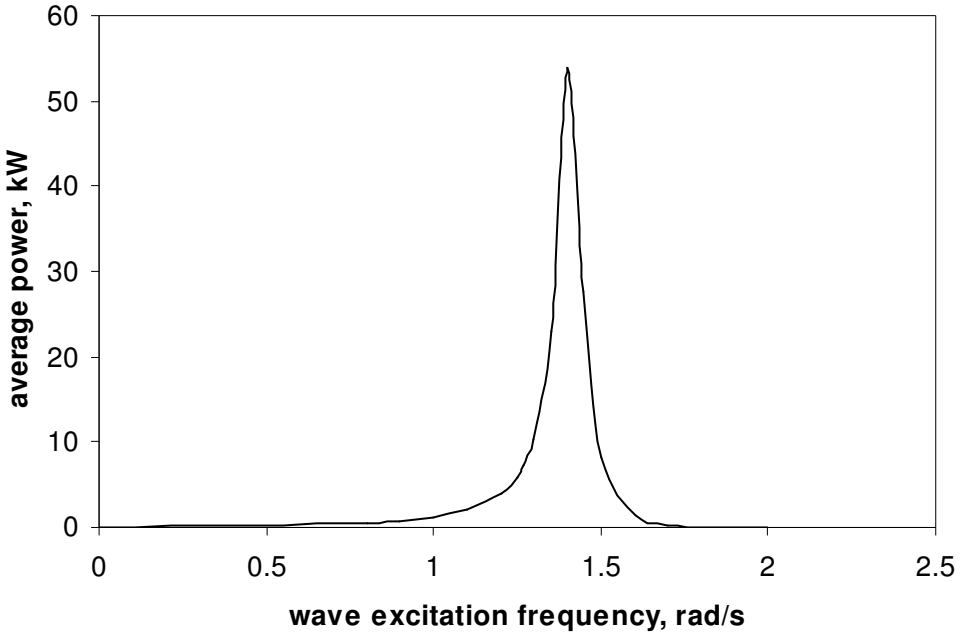

(a)

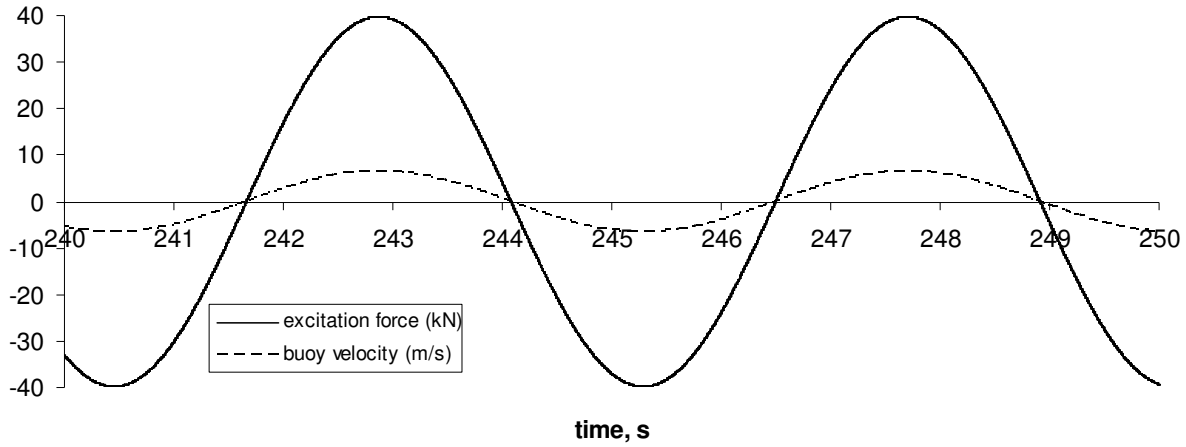
40
30
20
10
0
-10
-20
-30
-40
240
241
242
243
244
245
246
247
248
249
250
excitation force (kN)
buoy velocity (m/s)
time, s

(b)

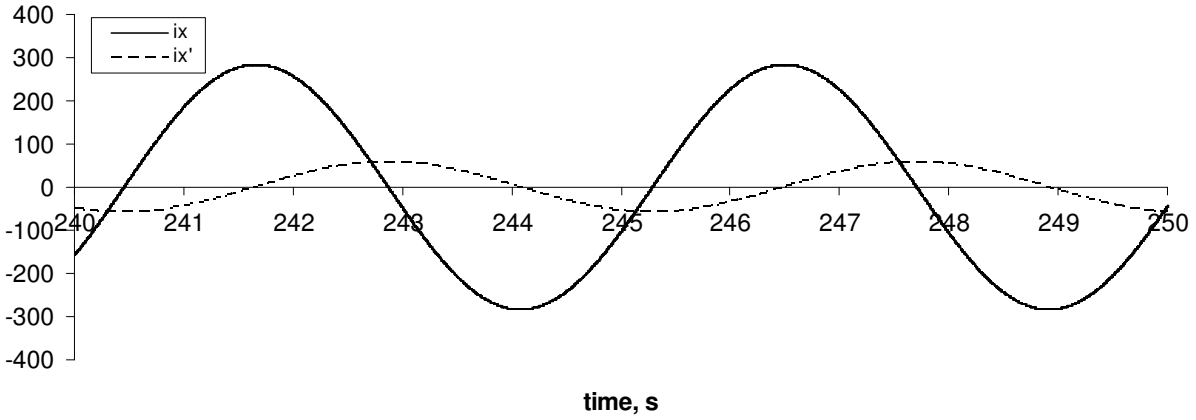
400
300
200
100
0
-100
-200
-300
-400
240
241
242
243
244
245
246
247
248
249
250
ix
ix'
time, s

(c)

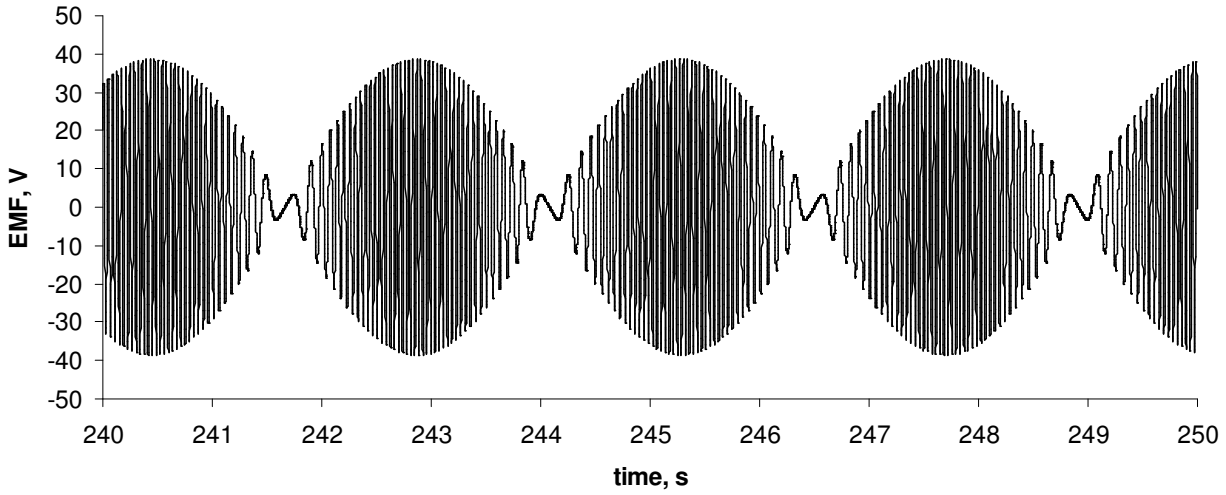
50
40
30
20
10
0
-10
-20
-30
-40
-50
240
241
242
243
244
245
246
247
248
249
250
EMF, V
time, s

(d)

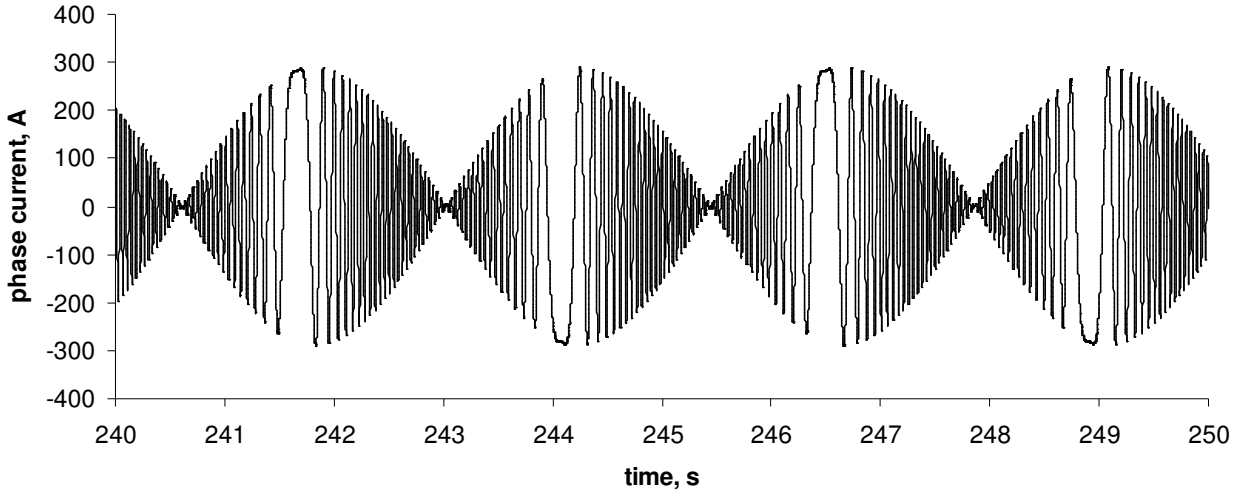

(e)

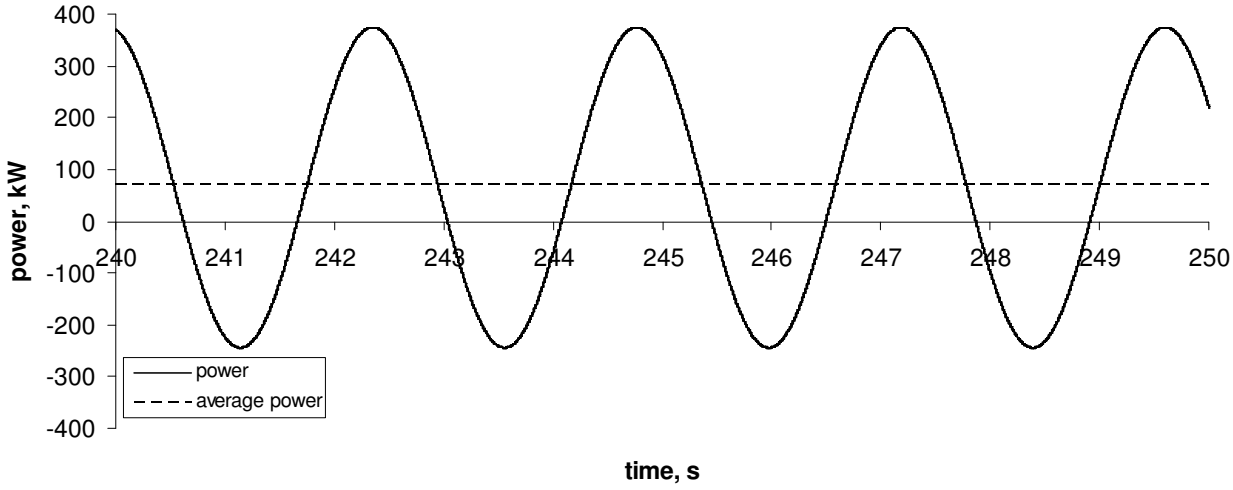

(f)

Fig. 10 (a)WEC frequency response, (b) Wave excitation force and buoy velocity, (c) i_x and $i_{\dot{x}}$ (d) Induced EMF for a single phase, (e) Armature current for a single phase, and (f) Generator instantaneous and average power

6 Discussion

As shown in Fig. 10(a) a heaving buoy wave energy converter has a highly resonant power-frequency characteristic. It should also be noted that the resonant frequency is high reflecting the fact that a smaller device has been modelled, which would operate closer to shore. In deep water a dominant wave period of approximately 10 seconds can be expected. The device would be designed so that the resonant frequency corresponds to the most common wave frequency at the site, but the device should also be controllable so that it can capture energy at frequencies either side of the resonant. In this paper it has been shown that an effective generator spring stiffness can be controlled to modify the overall stiffness of the system and hence the resonant frequency of the device. However, in order to do this, a

mechanical reactive force is required, which is produced by current i_x. As the results in Fig. 10(c) show, this current component is significantly larger than the damping current $i_{\dot{x}}$, which produces the useful active power. This mechanical reactive force leads to a negative power flow as shown in Fig. 10(f). Frequency control of the device therefore, requires a reactive power flow to supply a mechanical reactive force. It should be stressed that this is not the same as electrical reactive power, although its presence has the same impact in that the electrical generator and converter would have to be overrated in order to achieve the results shown in Fig. 10. It is apparent that mechanical methods for achieving phase control, such as latching, would require similar amounts of energy.

A flatter device frequency characteristic would be more suitable for phase control and lead to fewer problems in terms of sizing the machine. It has been shown by Salter that an inclining IPS buoy can lead to a wider bandwidth of energy capture, which makes control significantly less energy intensive [18]. For the purposes of illustration, the heaving buoy example used in this paper is very illuminating in subsequent issues associated with implementing phase control. The issue of machine sizing is also worth discussing. Even without any control the system needs to be sized according to the peak wave power that it is likely to encounter, which can be 5 times the average incident power. For example, the AWS device was peak rated at 2 MW with an average of 400 kW. The ratio of peak-to-average power shown in Fig. 10(f) is of a similar order to that of the AWS. Since the variation of power takes place over several seconds, there is opportunity for some cooling to take place. In real sea states the variation in power capture is much more random than in pure monochromatic seas states. Hence, there is some scope for investigating overload performance for machines in this application. Overrating generation equipment is an issue for wave energy systems as a whole, not just those using phase control. However, by applying phase control to a device with wider bandwidth further increases in rating size can be alleviated. An investigation into machine sizing and overload performance is forming the basis of future work, with the model and results presented in this paper providing the basis for the research.

7 Conclusions

The work presented in this paper has highlighted two aspects of a linear generator for direct drive wave energy conversion: control for maximum energy capture and linear generator force development using a simple analytical method. Theoretic analysis methods for a direct drive WEC are systematically provided, with both EMF and reaction forces of the VRPM machine verified by simulation. The simulation results show that while the proposed control system is feasible for implementation, the linear machine and power converter would have to be considerably overrated due to the reactive power demands. Control through electrical means, however, still represents an attractive option for a

direct drive system mainly due to its simplistic approach with other advantages to be realised through the course of ongoing investigation.

8 Acknowledgements

The authors would like to thank the Engineering and Physical Sciences Research Council for providing financial assistance. The authors would also like to acknowledge the support of the Scottish Funding Council for the Joint Research Institute with the Heriot-Watt University which is a part of the Edinburgh Research Partnership.

9 References

1. Energy White Paper: Our energy future - creating a low carbon economy, Department of Trade and Industry, February 2003
2. World Offshore Renewables Report 2004 - 2008, Department of Trade and Industry, 2004
3. Mueller, M.A. 'Electrical generators for direct drive wave energy converters', *IEE Proc. C Gener. Transm. Distrib.*, 2002, **149**, (4), pp. 446-456.
4. Baker, N.J., Mueller, M.A., and Brooking, P.R.M.: 'Electrical power conversion in direct drive wave energy converters'. European Wave Energy Conf., Cork, Ireland, 2003, pp. 197-204
5. Polinder, H, Mecrow, B.C., Jack, A.G., Dickinson, P., and Mueller, M.A.: 'Linear generators for direct-drive wave energy conversion'. IEEE Int. Elec. Machines and Drives Conf., Madison, Wisconsin, USA, 2003, **2**, pp. 798-804.
6. Falnes, J.: 'Optimum control of oscillation of wave-energy converters', Annex Report B1 to the JOULE project "Wave Energy Converters: Generic Technical Evaluation Study", 1993, Paper no. 2, JOU2-0003-DK
7. Korde, U.A.: 'Control system applications in wave energy conversion'. OCEANS 2000 MTS/IEEE Conf. and Exhib., 2000, **3**, pp. 1817-1824
8. Greenhow, M., and White, S.P.: 'Optimal heave motion of some axisymmetric wave energy devices in sinusoidal waves', *Applied Ocean Research*, 1997, **19,** (3-4), pp. 141-159.
9. Thomas, G.P.: 'Dimensional analysis applied to electricity and mechanics', *Physics Education.* 1979, **14**, (2), pp. 116-120.
10. Spooner, E., and Haydock, L.: 'Vernier hybrid machines', *IEE Proc. B Elec. Power App.* 2003, **150**, (6), pp. 655-662.
11. Spooner, E., Tavner, P., Mueller, M.A, and Baker, N.J.: 'Vernier hybrid machines for compact drive applications'. IEE Int. Conf. Power Electronics, Machines and Drives, Edinburgh, UK, 2004, pp. 452-457
12. Brooking, P.R.M, and Mueller, M.A.: 'Power conditioning of the output from a linear vernier hybrid permanent magnet generator for use in direct drive wave energy converters', *IEE Proc. C Gener. Transm. Distrib.* 2005, **152**, (5), pp. 673-681.
13. Eidsmoen, H.: 'Hydrodynamic parameters for a two-body axisymmetric system', *Applied Ocean Research*, 1995, **17**, (2), pp. 103-115.
14. Mueller, M.A., Xiang, J., Baker, N.J., and Brooking, P.R.M.: 'Dynamic modelling of a linear vernier hybrid permanent magnet machine coupled to a wave energy emulator test rig'. Int. Conf. Electrical Machines, Cracow, Poland, 2004
15. Mueller, M.A., and Baker, N.J.: 'Modelling the performance of the vernier hybrid machine', *IEE Proc. B Elec. Power App.* 2003, **150**, (6), pp. 647-654.
16. Iwabuchi, N., Kawahara, A., Kume, T., Kabashima, T., and Nagasaka, N.: 'A novel high-torque reluctance motor with rare-earth magnet', *IEEE Trans. Ind. App.* 1994, **30**, (3), pp. 609-614.
17. Freeman, E.M.: 'The calculation of harmonics, due to slotting, in the flux-density waveform of a dynamo-electric machine', *IEE Proc. Part C*, 1962, **109**, (16), pp. 581-588.
18. Salter, S.H., and Lin, C.P.: 'Wide Tank Efficiency Measurements on a Model of the Sloped IPS Buoy'. European Wave Energy Conf., Patras, Greece, 1998, pp. 200-206